

Directive emission of red conjugated polymer embedded within zero index metamaterials

Tun Cao,^{1,*} Yang Zou,¹ Ali M. Adawi² and Martin J. Cryan^{3,4}

¹Department of Biomedical Engineering, Dalian University of Technology, Dalian 116024, China (P.R.C)

²Department of Physics and Mathematics, University of Hull, Cottingham Road, HU6 7RX, Hull, UK

³Department of Electrical and Electronic Engineering, University of Bristol, Bristol, UK

⁴m.cryan@bristol.ac.uk

^{*}caotun1806@dlut.edu.cn

Abstract: We numerically demonstrate an impedance-matched multilayer stacked fishnet metamaterial that has zero index with flat high transmittance from 600nm to 620nm. The effective refractive index(n_{eff}) is calculated to be $-0.045+0.466i$ and the normalized effective impedance(Z_{eff}/Z_0) is $0.956-0.368i$ at 610nm. The light emitted by a red conjugated polymer layer embedded in such a zero index metamaterial (ZIM) is concentrated in a narrow cone in the surrounding media, where the half-power beam width (HPBW) of the center lobe of the radiation pattern is around 25° in the wavelength range between 600nm and 620nm, giving directive emission in the visible region. This proposed light focusing system can be applied to sensing, beam collimating and filtering functionalities.

OCIS codes: (160.3918) Metamaterials; (350.5610) Radiation.

References and links

1. J. B. Pendry, "Negative Refraction Makes a Perfect Lens," *Phys. Rev. Lett.* **85**, 3966-3969 (2000).
2. R. A. Shelby, D. R. Smith, and S. Schultz, "Experimental Verification of a Negative Index of Refraction," *Science* **292**, 77-79 (2001).
3. D. Schurig, J. J. Mock, B. J. Justice, S. A. Cummer, J. B. Pendry, A. F. Starr, and D. R. Smith, "Metamaterial Electromagnetic Cloak at Microwave Frequencies," *Science* **314**, 977-980 (2006).
4. T. Cao, C. Wei, R. Simpson, L. Zhang, and M. Cryan, "Rapid phase transition of a phase-change metamaterial perfect absorber," *Opt. Mater. Express* **3**, 1101-1110(2013).
5. T. Cao, R. Simpson, and M. Cryan, "Study of tunable negative index metamaterials based on phase-change materials," *J. Opt. Soc. Am. B* **30**, 439-444(2013).
6. M. A. Antoniades, and G. V. Eleftheriades, "A broadband series power divider using zero-degree metamaterial phase-shifting lines," *IEEE Microw. Wirel. Co.* **15**, 808-810(2005).
7. R. Liu, Q. Cheng, T. Hand, J. J. Mock, T. J. Cui, S. A. Cummer, and D. R. Smith, "Experimental Demonstration of Electromagnetic Tunneling Through an Epsilon-Near-Zero Metamaterial at Microwave Frequencies," *Phys. Rev. Lett.* **100**, 023903 (2008).
8. X. Huang, Y. Lai, Z. H. Hang, H. Zheng, and C. T. Chan, "Dirac cones induced by accidental degeneracy in photonic crystals and zero-refractive-index materials," *Nature Mater.* **10**, 582-586 (2011).
9. D. C. Adams, S. Inampudi, T. Ribaudou, D. Slocum, S. Vangala, N. A. Kuhta, W. D. Goodhue, V. A. Podolskiy, and D. Wasserman, "Funneling Light through a Subwavelength Aperture with Epsilon-Near-Zero Materials," *Phys. Rev. Lett.* **107**, 133901 (2011).
10. Y. Liu, L. He, L. Dong, L. Liu, Y. Shi, and C. Yang, "Multi-channelled filtering properties of the sandwich structures composed of epsilon-negative metamaterials," *J. Appl. Phys.* **114**, 063105 (2013).
11. S. Kocaman, M. S. Aras, P. Hsieh, J. F. McMillan, C. G. Biris, N. C. Panoiu, M. B. Yu, D. L. Kwong, A. Stein, and C. W. Wong, "Zero phase delay in negative-refractive-index photonic crystal superlattices," *Nat. Photonics* **5**, 499-505 (2011).
12. Q. Cheng, W. X. Jiang, and T. J. Cui, "Spatial power combination for omnidirectional radiation via anisotropic metamaterials," *Phys. Rev. Lett.* **108**, 213903 (2012).
13. W. Zhu, I. D. Rukhlenko, and M. Premaratne, "Light amplification in zero-index metamaterial with gain inserts," *Appl. Phys. Lett.* **101**, 031907 (2012).

14. S. Enoch, G. Tayeb, P. Sabouroux, N. Guerin, and P. Vincent, "A metamaterial for directive emission," *Phys. Rev. Lett.* **89**, 213902 (2002).
 15. W. Zhu, L. Si, and M. Premaratne, "Light focusing using epsilon-near-zero metamaterials," *AIP Adv.* **3**, 112124 (2013).
 16. V. Mocella, S. Cabrini, A. S. P. Chang, P. Dardano, L. Moretti, I. Rendina, D. Olynick, B. Harteneck, and S. Dhuey, "Self-Collimation of Light over Millimeter-Scale Distance in a Quasi-Zero-Average-Index Metamaterial," *Phys. Rev. Lett.* **102**, 133902 (2009).
 17. N. M. Litchinitser, A. I. Maimistov, I. R. Gabitov, R. Z. Sagdeev, and V. M. Shalaev, "Metamaterials: electromagnetic enhancement at zero-index transition," *Opt. Lett.* **33**, 2350–2352 (2008).
 18. P. Moitra, Y. Yang, Z. Anderson, Ivan I. Kravchenko, D. P. Briggs, and J. Valentine, "Realization of an all-dielectric zero-index optical metamaterial," *Nat. Photonics* **7**, 791–795 (2013).
 19. S. Yun, Z.H. Jiang, Q. Xu, Z.W. Liu, D.H. Werner, and T.S. Mayer, "Low-Loss Impedance-Matched Optical Metamaterials with Zero-Phase Delay," *ACS Nano* **6**, 4475–4482 (2012).
 20. Z.H. Jiang, L. Lin, J.A. Bossard, and D.H. Werner, "Bifunctional plasmonic metamaterials enabled by subwavelength nano-notches for broadband, polarization-independent enhanced optical transmission and passive beam-steering," *Opt. Express* **21**, 31492–31505 (2013).
 21. A.M. Adawi, L.G. Connolly, D.M. Whittaker, D.G. Lidzey, E. Smith, M. Roberts, F. Qureshi, C. Foden and N. Athanassopoulou, "Improving the light extraction efficiency of red-emitting conjugated-polymer light emitting diodes," *J. Appl. Phys.* **99**, 054505 (2006).
 22. M. Kafesaki, I. Tsiapa, N. Katsarakis, Th. Koschny, C. M. Soukoulis, and E. N. Economou, "Left-handed metamaterials: The fishnet structure and its variations," *Phys. Rev. B* **75**, 235114 (2007).
 23. J. Valentine, S. Zhang, T. Zentgraf, E. Ulin-Avila, D. A. Genov, G. Bartal, and X. Zhang, "Three-dimensional optical metamaterial with a negative refractive index," *Nature*, **455**, 376–379 (2008).
 24. Y.L. Zhang, W. Jin, X.Z. Dong, Z.S. Zhao, and X.M. Duan, "Asymmetric fishnet metamaterials with strong optical activity," *Opt. Express* **20**, 10776–10787 (2012).
 25. S. S. Kruk, D. A. Powell, A. Minovich, D. N. Neshev, and Y. S. Kivshar, "Spatial dispersion of multilayer fishnet metamaterials," *Opt. Express* **20**, 15100–15105 (2012).
 26. S. Zhang, W. Fan, N. C. Panou, K. J. Malloy, R. M. Osgood, and S. R. Brueck, "Optical negative-index bulk metamaterials consisting of 2D perforated metal-dielectric stacks," *Opt. Express* **14**, 6778–6787 (2006).
 27. N. Liu, Hongcang Guo, Liwei Fu, Stefan Kaiser, Heinz Schweizer, and Harald Giessen, "Three-dimensional photonic metamaterials at optical frequencies," *Nature Mater.*, **7**, 31–37 (2008).
 28. T. Li, H. Liu, F. M. Wang, Z. G. Dong, S. N. Zhu, and X. Zhang, "Coupling effect of magnetic polariton in perforated metal/dielectric layered metamaterials and its influence on negative refraction transmission," *Opt. Express* **14**, 11155–11163 (2006).
 29. C. García-Meca, J. Hurtado, J. Martí, A. Martínez, W. Dickson, and A. V. Zayats, "Low-loss multilayered metamaterial exhibiting a negative index of refraction at visible wavelengths," *Phys. Rev. Lett.* **106**, 067402 (2011).
 30. A. Rosenberg, K. Bussmann, M. Kim, M. W. Carter, M. A. Mastro, R. T. Holm, R. L. Henry, J. D. Caldwell, and C. R. Eddy Jr., "Fabrication of GaN suspended photonic crystal slabs and resonant nanocavities on Si(111)," *J. Vac. Sci. Technol. B* **25**(3), 721 (2007).
 31. J. J. Wierer, Jr., A. David, and M. M. Megens, "III-nitride photonic-crystal light-emitting diodes with high extraction efficiency," *Nat. Photonics* **3**(3), 163–169 (2009).
 32. Y. Wang, F. Hu, H. Sameshima, and K. Hane, "Fabrication and characterization of freestanding circular GaN gratings," *Opt. Express* **18**, 773–779 (2010).
 33. Y. Akihama and K. Hane, "Single and multiple optical switches that use freestanding silicon nanowire waveguide couplers," *Light: Sci. Appl.* **1**, 1–8 (2012).
 34. P. B. Johnson and R. W. Christy, "Optical Constants of the Noble Metals," *Phys. Rev. B* **6**, 4370–4379 (1972).
 35. R. W. Ziolkowski, "Design, fabrication, and testing of double negative metamaterials," *IEEE Trans. Antennas Propag.* **51**, 1516–1529 (2003).
 36. A. M. Nicolson and G. F. Ross, "Measurement of the intrinsic properties of materials by time domain techniques," *IEEE Trans. Instrum. Meas.* **19**, 377–382 (1970).
 37. D. R. Smith, S. Schultz, P. Markos, and C. M. Soukoulis, "Determination of Effective Permittivity and Permeability of Metamaterials from Reflection and Transmission Coefficient," *Phys. Rev. B* **65**, 195104 (2002).
 38. X. D. Chen, T. M. Grzegorzczak, B. Wu, J. Pacheco, Jr., and J. A. Kong, "Robust method to retrieve the constitutive effective parameters of metamaterials," *Phys. Rev. E* **70**, 016608 (2004).
 39. A. Fang, Z. Huang, T. Koschny, and C. M. Soukoulis, "Overcoming the losses of a split ring resonator array with gain," *Opt. Express* **19**, 12688–12699 (2011).
 40. A. Fang, Th. Koschny, M. Wegener, and C. M. Soukoulis, "Self-consistent calculation of metamaterials with gain," *Phys. Rev. B* **79**, 241104(R) (2009).
 41. J. D. Jackson, *Classical Electrodynamics, Second Edition* (John Wiley & Sons, 1975, pp.401).
-

1. Introduction

Metamaterials (MMs) have witnessed rapid developments since the pioneering works by Pendry *et al.*[1]. and Smith *et al.*[2]. As artificial structures, MMs offer a unique opportunity for manipulating the optical properties of matter, hence leading to a variety of exciting applications, including electromagnetic cloaks[3], perfect absorbers[4], negative refractive index[5] and zero phase delay lines[6]. Recently, zero index metamaterials (ZIMs) have attracted significant attention[7-15]. Light propagating through the ZIMs will be concentrated in a narrow cone in the surrounding media thus enhancing the directive emission. This property enables an array of new devices such as highly directive antennas[14], beam self-collimators[16] and electromagnetic field enhancers[17]. An epsilon-near-zero metamaterial (ENZM) was first experimentally demonstrated by Enoch *et al.*[14], which has an effective permittivity ϵ_{eff} near zero, leading to a near-zero effective refractive index $n_{\text{eff}} = \sqrt{\epsilon_{\text{eff}} \mu_{\text{eff}}}$, where μ_{eff} is the effective permeability of the structure. However, the effective impedance $Z_{\text{eff}} = \sqrt{\mu_{\text{eff}} / \epsilon_{\text{eff}}}$ of ENZM is mismatched to free space impedance $Z_0 = \sqrt{\mu_0 / \epsilon_0}$ as $Z_{\text{eff}} \rightarrow \infty$ with $\epsilon_{\text{eff}} \rightarrow 0$. This gives rise to large reflections from the interface[18]. Just recently Yun *et al.* have demonstrated an impedance-matched ZIM with nearly ideal transmission in the near-infrared region (N-IR), where both $n_{\text{eff}} \rightarrow 0$ and $Z_{\text{eff}} \rightarrow Z_0$ [19]. This has been achieved by making both ϵ_{eff} and μ_{eff} approach zero and their $\sqrt{\mu_{\text{eff}} / \epsilon_{\text{eff}}} \rightarrow Z_0$ within the desired optical range. Jiang *et al.* have numerically analyzed broadband impedance-matched ZIMs in the mid-infrared region (M-IR) using nano-notch loaded modified fishnet MMs[20]. Although great progresses have been made on impedance-matched ZIMs, the interest of exploring the light emission from an embedded source within such materials is rarely looked into. Most recently, Moitra *et al.* have experimentally presented impedance-matched ZIMs in the N-IR region based on purely dielectric constituents[18]. This structure enables a directive emission from quantum dots placed within the structure, showing a great promise for enhancing the emission directionality of a source embedded in the impedance-matched ZIMs. However, this research has focused on achieving a directive emission using all-dielectric ZIMs, which limits its application in MMs based on metal/dielectric layers. Moreover, most research has focused on demonstrating ZIMs in the microwave, M-IR and N-IR regions. Whereas, modifying the radiation of an embedded source within impedance-matched ZIMs in the visible region has yet to be shown. In this work, we study for the first time to our knowledge, impedance- matched ZIMs with embedded red conjugated polymer emitting that has been utilized in light-emitting diodes[21] and when optically pumped is able to undergo lasing.

Recently, the achievements of the multilayer fishnet MMs have established a promising approach for a three dimensional(3D) optical MMs and become a strong candidate for nearly all possible applications[22-28]. Therefore, here The design of the ZIM is developed from a low loss multilayered fishnet MM exhibiting a negative refractive index in the visible region[29]. Our proposed structure has a configuration of a round nanohole array (RNA) embedded through a vertically stacked Metal-Dielectric-Metal multilayer, in which the red polymer layer is located in the center of the structure as an emitting source. The resulting device offers near zero ϵ_{eff} and μ_{eff} , thus leading to a near zero n_{eff} and $Z_{\text{eff}} \rightarrow Z_0$ with a flat high transmittance from 600nm to 620nm due to the focusing effect in the ZIM[14]. The Finite Difference Time Domain (FDTD) method is used to show evidence of impedance-matched near-zero n_{eff} within the structure and illustrates the focusing performance of the system. This proposed light focusing system will find applications in sensing, beam collimating, filtering and directional light sources operating in the visible region. The fabrication of this multilayer structure may sound challenging, but leveraging off the rapid developments in optical and

interferometric lithography, in nanoimprinting and in nanoscale self-assembly techniques, fabrication of this structure should be feasible, i.e. for a proof of concept focused ion beam(FIB) can be used to fabricate these structures as in ref. 29 or even electron beam lithography(EBL) and selective etching using reactive ion etching with different gases.

2. Metamaterials design

The proposed ZIM consists of a multilayer stack of 11 alternating layers of 35nm thick Au and 30nm thick dielectric layer with an inter-penetrating two dimensional square array of round holes shown in Fig. 1(a), in which a 30nm thick red polymer layer is placed in the center of the ZIM. The refractive index of the dielectric layer is 1.41 [29].The unit cell is shown in Fig. 1(b), where the lattice constant of the holes is $L=400\text{nm}$, the diameter of the holes is $d=240\text{nm}$ which have been optimized to exhibit an impedance-matched zero index within the emission band of the embedded conjugated polymer. The isotropic round holes periodically extended along the x and y axes with identical periodicity. The z -axis is normal to the structure surface and the x - y plane is parallel to the structure surface. In order to simplify the design, the structures are considered to be suspended in vacuum; deep etching of a silicon support substrate can be used to achieve this [30-33]. Au is selected as the metal due to its stability and low ohmic loss. The dielectric properties of Au as given by Johnson & Christy are used[34]. The red polymer material was selected due to its visible emission. The real $n_s(\omega)$ and imaginary $k_s(\omega)$ parts of the refractive index for the red polymer material were obtained from the published data in ref. 21. A commercial software Lumerical FDTD Solutions is used to calculate the S -parameters corresponding to the frequency dependent reflection $r(\omega)$ and transmission $t(\omega)$ coefficients of the structure, which are then taken to retrieve the so-called material parameters ϵ_{eff} , μ_{eff} and n_{eff} of the ZIMs using the well-known Nicholson-Ross-Weir (NRW) method[35,36]. The structure is excited with a plane wave source in the center of red polymer layer, which is sandwiched between the third and fourth Au layers within the structure. The computational domain ($400\text{ nm} \times 400\text{ nm} \times 1000\text{ nm}$) has perfectly match layer and absorbing boundaries in the z direction and periodic boundaries in the x - y plane. A uniform FDTD mesh size is adopted; the mesh size is the same along all Cartesian axes: $\Delta x = \Delta y = \Delta z = 2\text{ nm}$, which is sufficient to minimize the numerical errors arising from the FDTD method.

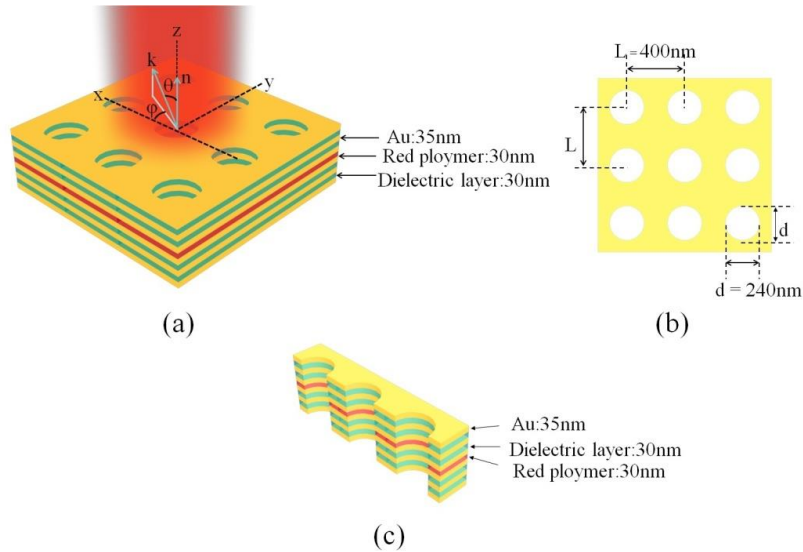


Fig. 1. (a) Diagram of the ZIM consisting of a multilayer stack of 11 alternating layers of 35nm thick Au and 30nm thick dielectric layer with an inter-penetrating two dimensional square array of round holes. The structure is suspended in a vacuum. The lattice constant is $L=400\text{nm}$ and hole diameter is $d=240\text{nm}$. The light is emitted from a 30nm thick fluorescent polymer layer within the ZIM. (b) Illustration of round holes array lattice. (c) Scheme of the cross section of the structure.

3. Results and discussions

Figure 2 shows the transmittance ($T(\omega)$) and effective optical properties of the ZIM, FDTD simulations were used to calculate the complex transmission ($t(\omega)$) and reflection ($r(\omega)$) coefficients, which were then used in S-parameter retrieval[18], where $T(\omega) = |t(\omega)|^2$. Here we use the NRW method to perform the S-parameter retrieval procedure using the calculated normal incidence transmission and reflection coefficients[37,38]. In this case the transmittance is defined as the ratio of the power received in a plane 320nm above the structure to the emitted power from the centre of the polymer layer. This neglects downward emitted power, but is sufficient for a basic understanding the effect of the ZIM structure on emission. In future works we will use random arrays of dipole emitters which are a more realistic model for this type of emission. In Fig. 2(a), we can see that the transmittance remains high around 0.6 with both a broad and flat passband from 600 to 620nm. This flat passband corresponds to the impedance-matched near zero n_{eff} band (where $|Real(n_{\text{eff}})| < 0.267$) shown in Fig.2(b), the $Real(n_{\text{eff}})$ shows a smooth transition from 0.068 to -0.267 in the flat passband 600nm-620nm, and an almost zero value of n_{eff} ($n_{\text{eff}} = -0.045 + 0.466i$) is observed at 610nm. Regarding losses, the figure-of-merit (FOM) defined as $FOM = real(n_{\text{eff}}) / Imag(n_{\text{eff}})$ is taken to show the overall performance of the ZIM shown in Fig.2(d). The peak value of FOM is 1.18 at 620nm. It should be noted that the FOM could be further increased by using lower-loss metallic films, or incorporating gain materials into the structures [39-40]. As can be seen in Fig.2(c), within the passband the real part of ϵ_{eff} and μ_{eff} follow the near-zero values where $|Real(\epsilon_{\text{eff}})| < 0.8$ and $|Real(\mu_{\text{eff}})| < 0.8$, hence enabling a good impedance-matched near zero n_{eff} band so that the majority of the light is emitted out of the structure.

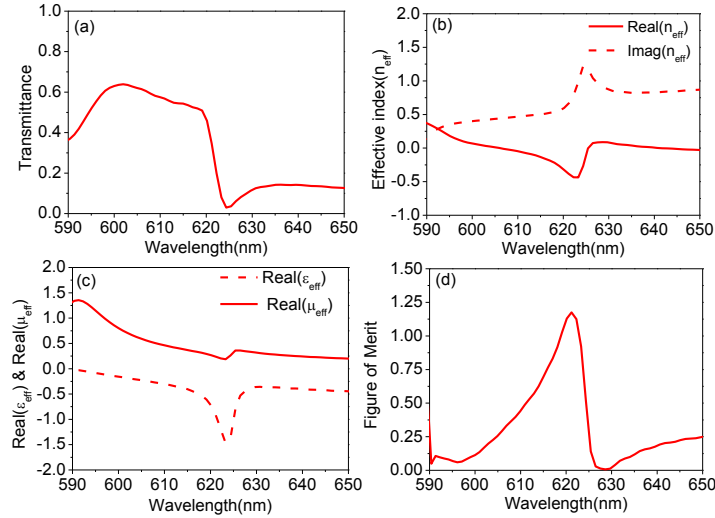


Fig. 2. (a) Theoretical transmittance curves of the ZIM. (b) The real part ($Real(n_{\text{eff}})$) and imaginary part ($Imag(n_{\text{eff}})$) of the effective refractive index of the ZIM obtained using S-

parameter retrieval.(c)The real part of the effective permittivity $Real(\mu_{eff})$ and permeability $Real(\mu_{eff})$ of the ZIM obtained using S-parameter retrieval. (d)Figure-of-merit of the ZIM.

Figure 3 shows that the near-unity normalized effective impedance(Z_{eff} / Z_0) with a small imaginary part can be obtained throughout the passband owing to the good impedance match to free space, hence providing a high transmittance across the band. The value of Z_{eff} / Z_0 is $0.956-0.368i$ at 610nm.

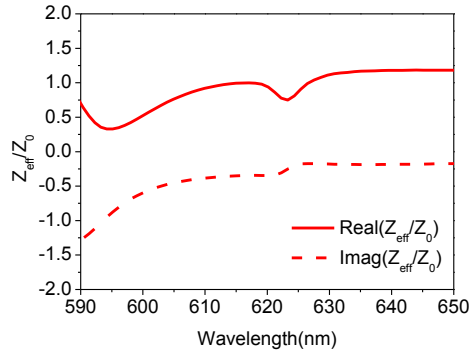


Fig. 3. The real and imaginary parts of the effective impedance of the ZIM.

For this type of ZIM, the transmittance is also robust for non-normal angles of incidence. In Fig.4, we examine the transmittance versus wavelength and angle of incidence. It shows that the transmittance simply reduces as the angle of incidence increases, and allows a broad and flat transmittance larger than 40% at 40° within near zero index region. Therefore, this proposed structure is a low loss impedance-matched ZIM over a wide range of incident angles in the visible region.

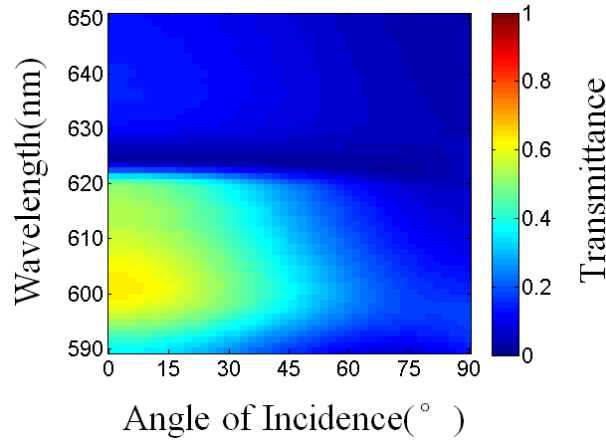


Fig. 4. Simulated angle- and wavelength-dependent transmittance of the ZIM.

Isotropic emitters placed within the ZIM are expected to emit almost entirely along the direction normal to the air-ZIM interface[14,18]. To demonstrate this effect, Fig. 5 shows the emission diagram from a plane wave source in the center of the ZIM, in which the source emits at a central wavelength sweeping from 590 to 650nm. A portion of the structures with a length

of one unit cell in the x direction and a width of one unit cell in the y direction was considered. To mimic a two dimensionally infinite structure, periodic boundary conditions were assigned in the in the x - y plane[14,20]. The perfectly match layer boundary condition is set along the z direction. Here, a standard procedure in Lumerical FDTD has been applied to simulate the far field radiation pattern of an antenna in free space[41]. In particular we sample the tangential fields above the structure then the far-field radiation patterns are extracted by projecting the scattered radiation in the near field to the far field. Namely, we calculate the far-field distribution from the near field information by doing the near-to-far field transformation. Figures 5 (b)-5(d) show the emission profile within the spectral range 600-620nm. As it can be seen the emission pattern is confined to a narrow lobe around the normal of the structure with a half-power beam width (HPBW) around 25° . The two small side lobes at 30° and 150° are due to scattering from the corners of the ZIM[18]. Outside the passband, the emission of the structure cannot be concentrated to an overall angular spread hence leading to a lower transmittance as can be seen in Figs.5(a) and 5(e)-5(g). This confirms the directivity enhancement of the proposed ZIM in the visible region.

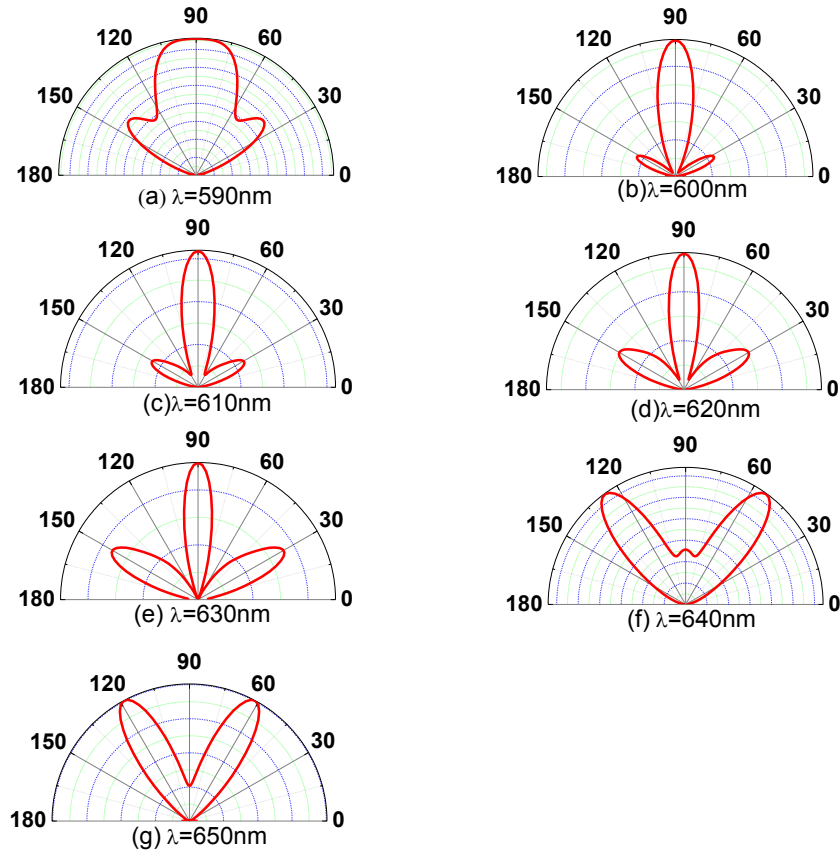


Fig. 5. Calculated emission profile for a plane wave source placed in the middle of the ZIM at center wavelengths of (a)590nm (b)600nm (c)610nm (d)620nm (e)630nm (f)640nm (g)650nm.

In order to further justify the fact that directivity enhancement is mainly induced by the ZIM, we have simulated the emission profile of two reference structures. The first reference structure is a 30 nm flat layer of the red polymer as illustrated in Fig. 6(a). The second reference

structure consists of a 30 nm thick layer of the red polymer that contains a square lateral pattern identical to the ZIM structure as illustrated in Fig. 6(b). The proposed multilayer ZIM is shown in Fig. 6(c). The emission patterns for a plane source placed in the middle of the different structures are demonstrated together with the structural schemes respectively, at the central wavelength of 610nm. As can be seen, the emission profile from the single flat red polymer layer and the RNA embedded through the single red polymer layer focus the light less efficiently than the ZIM owing to the absence of the zero index region. HPBW of the lobes are 44° for the flat layer of the red polymer and 42° for the red polymer layer embedded with the RNA. However, the HPBW of the lobe is 25° for the ZIM.

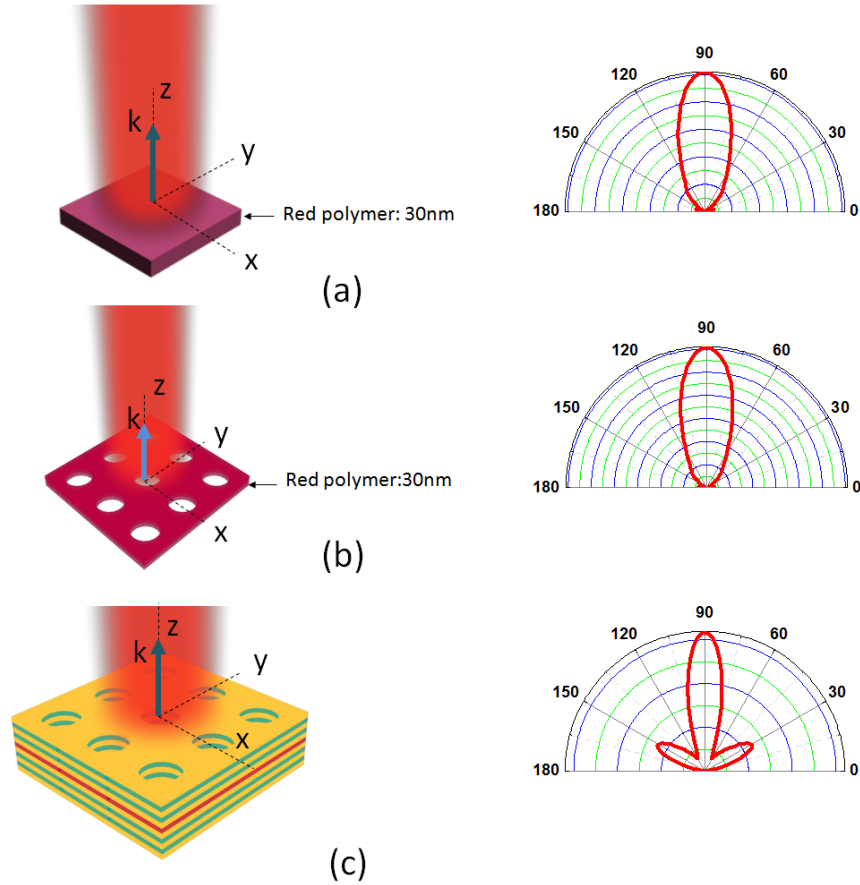


Fig. 6. (a) Illustration of a 30nm flat red polymer layer without holes; calculated emission profile for a plane source placed in middle of the 30nm thick single polymer layer at the central wavelength of 610nm. (b) Illustration of the round nanoholes array ($L=400\text{nm}, d=240\text{nm}$) embedding through a 30nm thick single red polymer layer; calculated emission profile for a plane source placed in middle of the 30nm thick single polymer layer at the central wavelength of 610nm. (c) Illustration of the round nanoholes array ($L=400\text{nm}, d=240\text{nm}$) embedding through a multilayer stack of 11 alternating layers of 35nm thick Au and 30nm thick dielectric layer; calculated emission profile for a plane source placed in middle of the ZIM at the central wavelength of 610nm.

4. Conclusions

In conclusion, a low loss impedance-matched stacked fishnet ZIM in the visible region has been investigated by FDTD simulation. Particularly, such a multilayer ZIM exhibits a flat passband from 600nm to 620nm with a high transmittance over a wide incident angle. This

entails an important step towards the control of the direction of emission of a source embedded within the ZIM. This work will open new avenues towards the development of directional light sources, beam self-collimators and electromagnetic field enhancers.

Acknowledgments

We acknowledge the financial support from National Natural Science Foundation of China (Grant No. 61172059, 51302026), Ph.D Programs Foundation of Ministry of Education of China (Grant No. 20110041120015), Postdoctoral Gathering Project of Liaoning Province (Grant No. 2011921008), and The Fundamental Research for the Central University (Grant No. DUT14YQ109).